

## Relativistic hybrid stars with sequential first-order phase transitions in light of multimessenger constraints

JIA JIE LI,<sup>1</sup> ARMEN SEDRAKIAN,<sup>2,3</sup> AND MARK ALFORD<sup>4</sup>

<sup>1</sup>*School of Physical Science and Technology, Southwest University, Chongqing 400715, China*

<sup>2</sup>*Frankfurt Institute for Advanced Studies, D-60438 Frankfurt am Main, Germany*

<sup>3</sup>*Institute of Theoretical Physics, University of Wrocław, 50-204 Wrocław, Poland*

<sup>4</sup>*Department of Physics, Washington University, St. Louis, MO 63130, USA*

### ABSTRACT

In this work, we consider the properties of compact stars in which quark matter has low- and high-density phases that are separated by a first-order phase transition. Thus, unlike the commonly considered case of a single phase transition from hadronic to quark matter, our models of hybrid stars contain sequential phase transitions from hadronic matter to low- and then to high-density quark matter phases. We extend our previous study of the parameter space of hybrid stars with a single phase transition to those with sequential phase transitions, taking into account the constraints on the mass and radius of neutron stars from the NICER experiment, the experimental inferences of the neutron skin thickness of the lead nucleus by the PREX-II experiment, and constraints on the tidal deformability from the gravitational-wave event GW170817. We determine the range of the masses for which both twin and triplet configurations, i.e., identical-mass stars with two and three different values of radii, arise.

*Keywords:* Neutron stars (1108); Neutron star cores (1107); Nuclear astrophysics (1129); High energy astrophysics (739); Gravitational waves astronomy (675)

### 1. INTRODUCTION

The possibility of phase transition from hadronic to quark matter and its implications for the properties of compact stars (CSs) has been the focus of researchers since early work on the subject several decades ago (Ivanenko & Kurdgelaidze 1965; Itoh 1970; Collins & Perry 1975); for recent reviews, see Alford et al. (2008); Anglani et al. (2014); Pisarski et al. (2019). An interesting special case is the possibility of a first-order phase transition between the hadronic and quark phases, which occurs when mixed phases are disfavored by surface tension and electrostatic energy costs (Alford et al. 2001). It has been established since that the first-order phase transition leads to a softening of the equation of state (EoS) and lower maximum masses of the sequences of hybrid stars compared to their purely hadronic counterparts. In a previous paper (Li et al. 2021b) we studied the implications of the recent radius determination of PSR J0740+6620 by the NICER experiment and the determination of the neutron skin by the PREX-II experiment (which gives information about symmetry energy and its slope) for the structure of hybrid stars with a strong first-order phase transition from nucleonic to quark matter. It was argued that if the interpretation of the PREX-II experiment implies a stiff EoS, and hence a large radius

for the nucleonic branch, an early first-order phase transition may relax the tensions with the astrophysical inferences of radii for the relevant ranges of masses of CSs. We also deduced the ranges of mass and radius of twin stars which, however, were restricted to a relatively narrow domain of masses and radii.

The purpose of this work is to implement the idea of sequential first-order phase transitions in a hybrid star (Alford & Sedrakian 2017), in particular the case where there are two such transitions, which can be realized in Nambu–Jona-Lasinio (NJL) models (e.g., Blaschke et al. 2010; Bonanno & Sedrakian 2012; Klähn et al. 2013). Here, we will continue using the scheme developed in our previous work (Li et al. 2020a, 2021b) which accounts for the currently available multimessenger information coming from various channels of astronomical observations and terrestrial experiments. Let us give, at this point, a brief list of the constraints against which our models developed below will be tested:

- PSR J0030+0451: This is the first object with mass and radius inferred to a precision of around 10% (Riley et al. 2019; Miller et al. 2019). These quantities were extracted from the fits to the data coming from the NICER observatory, which required modeling the soft X-ray pulses produced by the stellar rotation and the hot spots on the star’s surface and fitting to the waveforms. The two (independent) analyses predict (68% credible interval)  $M = 1.34^{+0.15}_{-0.16} M_{\odot}$ ,

$R = 12.71^{+1.14}_{-1.19}$  km (Riley et al. 2019) and  $M = 1.44^{+0.15}_{-0.14} M_{\odot}$ ,  $R = 13.02^{+1.24}_{-1.06}$  km (Miller et al. 2019).

- PSR J0740+6620: The mass of this pulsar was initially measured (Cromartie et al. 2020) using Shapiro delay to be  $2.08^{+0.07}_{-0.07} M_{\odot}$ . Its mass and radius were determined using the NICER X-ray light curves with the results for the radius  $12.39^{+1.30}_{-0.98}$  (Riley et al. 2021) and  $13.71^{+2.61}_{-1.50}$  km (Miller et al. 2021) and corresponding mass estimates  $2.07^{+0.07}_{-0.07} M_{\odot}$  and  $2.08^{+0.09}_{-0.09} M_{\odot}$  (68% credible interval).
- GW170817: The tidal deformability (TD) of a star of mass  $\sim 1.4 M_{\odot}$  in the GW170817 event by the LIGO-Virgo Collaboration (Abbott et al. 2017, 2018, 2019) was constrained to be below the (dimensionless) value  $\Lambda_{1.4} \leq 580$ , which implies a soft EoS at the intermediate (a few times nuclear saturation) density range. This observation is consistent with a phase transition from hadronic to quark matter, which can improve the agreement of theoretical models with the TD extracted from GW170817 event (e.g., Annala et al. 2018; Paschalidis et al. 2018; Most et al. 2018; Tews et al. 2018; Burgio et al. 2018; Alvarez-Castillo et al. 2019; Christian et al. 2019; Montana et al. 2019; Sieniawska et al. 2019; Essick et al. 2020; Li et al. 2020a; Miao et al. 2020; Li et al. 2021a; Malfatti et al. 2020; Rodriguez et al. 2021; Tan et al. 2022). Furthermore, the phase transition may lead to the emergence of new branches of stable CSs, which provides a new diagnostics of phase transition in CSs, through observation of *twin and triplet stars*, i.e., one or two hybrid stars having the same mass, but different radii from, a purely hadronic star (e.g., Alford et al. 2013; Alford & Sedrakian 2017; Paschalidis et al. 2018; Alvarez-Castillo et al. 2019; Christian et al. 2019; Montana et al. 2019; Li et al. 2020a; Christian & Schaffner-Bielich 2022).

Due to the high mass of PSR J0740+6620, it probes the region of densities that is highly relevant to a possible phase transition to quark matter. Recent work on the EoS has generally concluded, independent of the details of the EoS and methods of comparison with the multimessenger data adopted, that the EoS of the star must be moderately soft at intermediate densities and stiff enough at high densities. The first requirement accounts for the small TD in GW170817, while the second one accounts for the large mass of PSR J0740+6620 (e.g., Li et al. 2021b; Tan et al. 2022; Biswas 2022; Legred et al. 2021; Raaijmakers et al. 2021; Huth et al. 2022; Zhang & Li 2021; Tang et al. 2021; Christian & Schaffner-Bielich 2022; Jokela et al. 2022; Drischler et al. 2022; Contrera et al. 2022).

The isospin dependence of the nuclear interaction is constrained by the measurements of the neutron skin of nuclei. Most recently, the Lead Radius Experiment Collaboration (PREX-II) measured the neutron skin thickness of the lead nucleus,  $R_{\text{skin}}^{208} = 0.283 \pm 0.071$  fm (mean and  $1\sigma$  deviation), in a parity-violating electron-scattering experiment (Adhikari

et al. 2021). The existing theoretical analyses (Reed et al. 2021; Reinhard et al. 2021) do not converge to a consistent mean value of the symmetry energy,  $E_{\text{sym}}$ , and its slope,  $L_{\text{sym}}$ , at nuclear saturation density. While the first reference (Reed et al. 2021) infers  $E_{\text{sym}} = 38.1 \pm 4.7$  MeV and  $L_{\text{sym}} = 106 \pm 37$  MeV using a family of relativistic density functionals (DFs), the second reference (Reinhard et al. 2021) finds  $E_{\text{sym}} = 32 \pm 1$  MeV and  $L_{\text{sym}} = 54 \pm 8$  MeV using a larger number of relativistic and nonrelativistic DFs. (These two analyses are still consistent with each other at better than  $2\sigma$  accuracy.) They also included additional constraints from the experimental limits on the dipole polarizability of  $^{208}\text{Pb}$ , which prefer DFs predicting a small value of  $L_{\text{sym}}$  (Reinhard et al. 2021). While the second set of parameter values is within the standard range (Lattimer & Lim 2013; Danielewicz & Lee 2014; Oertel et al. 2017; Baldo & Burgio 2016), the first set is not. In particular, their large value of  $L_{\text{sym}}$  is in tension with the GW170817 deformability measurement if one assumes a purely nucleonic composition (Reed et al. 2021). Other authors (Essick et al. 2021) have confirmed the tension between the results of Reed et al. (2021) and astrophysical data using a nonparametric EoS. Thus, following our previous work (Li et al. 2021b), we will consider a broader range of  $L_{\text{sym}}$  to cover the possibilities claimed in the work above.

The physics of dense quark matter allows for multiple quark phases with distinct properties. One standard scenario is two-flavor color-superconducting (2SC) at medium densities and the color-flavor-locked (CFL) phase at high density. Thus, one of the aims of this work is to expand on the previous study (Li et al. 2021b), which was restricted to twin configurations, by considering triplets—three stars with the same mass but different radii—which can arise if there are three disconnected branches in the mass-radius (hereafter  $M$ - $R$ ) diagram (Alford & Sedrakian 2017; Li et al. 2020a).

The paper is organized as follows. In Section 2 we briefly define the EoS that we use to describe the hadronic and quark phases. In Section 3 we assess the existence of twin or triplet configurations and confront the resultant EoS models with the inferences from GW170817 and NICER observations of PSR J0740+6620. Our conclusions are given in Section 4.

## 2. CONSTRUCTION OF EQUATION OF STATE AND BASIC PICTURE

### 2.1. Nuclear matter equation of state

We will adopt for the hadronic phase the same description as in the predecessor paper (Li et al. 2021b). We provide below a brief account of our approach for the sake of completeness. The hadronic matter is described within a covariant density-functional (CDF) approach with density-dependent nucleon-meson couplings (Lalazissis et al. 2005). The density dependence of the coupling allows us to establish a one-to-one correspondence between our CDF and the purely phenomenological expansion of the energy density of nuclear matter (e.g., Margueron et al. 2018) in the vicinity of the saturation density,  $\rho_{\text{sat}}$ , with respect to the number density  $\rho$  and isospin asymmetry  $\delta = (\rho_n - \rho_p)/\rho$  where  $\rho_{n(p)}$  is

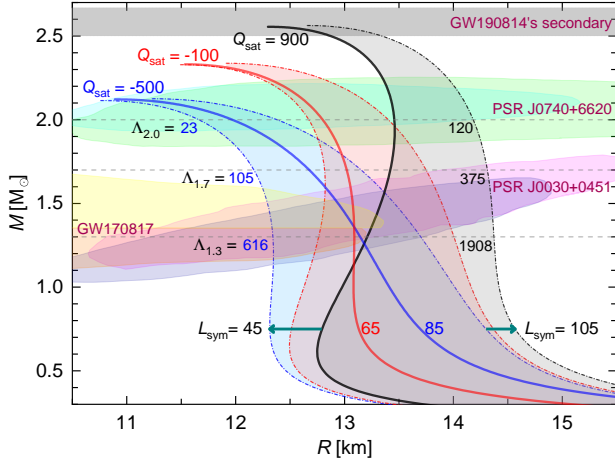


**Figure 1.**  $M$ - $R$  relation for nucleonic EoS within different pairs of values of  $Q_{\text{sat}}$  and  $L_{\text{sym}}$  (in MeV). We show three ranges of  $M$ - $R$  curves, for  $Q_{\text{sat}} = 900$  MeV (gray),  $-100$  MeV (red) and  $-500$  MeV (blue). For each,  $L_{\text{sym}}$  is varied from 45 MeV to 105 MeV. Thick solid lines show combinations of  $(Q_{\text{sat}}, L_{\text{sym}})$  that could marginally meet the GW170817 constraint, i.e.,  $(900, 45)$ ,  $(-100, 65)$ , and  $(-500, 85)$ . In addition, we show the TDs of CSs with mass  $M/M_{\odot} = 1.3, 1.7$ , and  $2.0$  for two extreme models. Constraints at 90% credibility from multimessenger astronomy are shown by shaded regions (Abbott et al. 2019; Riley et al. 2019, 2021; Miller et al. 2019, 2021); see text for details.

the neutron (proton) number density, as

$$E(\chi, \delta) \simeq E_{\text{sat}} + \frac{1}{2!} K_{\text{sat}} \chi^2 + \frac{1}{3!} Q_{\text{sat}} \chi^3 + E_{\text{sym}} \delta^2 + L_{\text{sym}} \delta^2 \chi + \mathcal{O}(\chi^4, \chi^2 \delta^2), \quad (1)$$

where  $\chi = (\rho - \rho_{\text{sat}})/3\rho_{\text{sat}}$ . The coefficients of this double expansion are referred to commonly as *incompressibility*,  $K_{\text{sat}}$ , the *skewness*,  $Q_{\text{sat}}$ , the *symmetry energy*,  $E_{\text{sym}}$ , and its *slope parameter*,  $L_{\text{sym}}$ . The mapping between the CDF and the phenomenological expansion (1) allows us to express the gross properties of CSs in terms of physically transparent quantities.

In this work, we use three sets of representative EoS models, taking three values of  $Q_{\text{sat}} = -500, -100$ , and  $900$  MeV, and exploring values of  $L_{\text{sym}}$  ranging from 45 to 105 MeV. Larger values of  $L_{\text{sym}}$  correspond to a stiffer EoS near nuclear saturation density, leading to larger radii for a  $1.4 M_{\odot}$  star. Larger values of  $Q_{\text{sat}}$  mean that the EoS is stiffer at high density, thereby increasing the maximum mass of a static nucleonic CS (e.g., Li & Sedrakian 2019; Zhang et al. 2018; Margueron et al. 2018). For  $Q_{\text{sat}} = -500$  MeV the maximum mass is about  $2.1 M_{\odot}$ , which matches the mass measurement of PSR J0740+6620 (Cromartie et al. 2020; Fonseca et al. 2021); for  $Q_{\text{sat}} = -100$  MeV the maximum mass is consistent with the (approximate) *upper limit* on the maximum mass of static CSs  $\sim 2.3 M_{\odot}$  inferred from the analysis of the GW170817 event (Rezzolla et al. 2018; Khadkikar et al. 2021); finally, for  $Q_{\text{sat}} = 900$  MeV the maximum mass is

close to  $2.5 M_{\odot}$ , which would be compatible with the mass of the secondary in the GW190814 event (Abbott et al. 2020b) and its interpretation as a nucleonic CS (Fattoyev et al. 2020; Sedrakian et al. 2020; Li et al. 2020b). We choose the range of  $L_{\text{sym}}$  between the central value and the lower limit of the 90% credible interval (CI) of the PREX-II measurement (Adhikari et al. 2021; Reed et al. 2021).

The  $M$ - $R$  relations for our nucleonic EoS models are shown in Figure 1, along with the current astrophysical observational constraints. These include (i) the ellipses obtained by the two NICER modeling groups for PSR J0030+0451 and J0740+6620 (Riley et al. 2019, 2021; Miller et al. 2019, 2021); (ii) the regions for each of the two CSs that merged in the gravitational-wave (GW) event GW170817 (Abbott et al. 2019); and (iii) the mass of the secondary component of GW190814 (Abbott et al. 2020b). All the regions/limits are given at 90% CI. As seen from Figure 1, the softness of the EoS (as implied by the GW170817 event) and stiffness at low and intermediate densities implied by the large value of  $L_{\text{sym}}$  suggested by one of the analyses (Reed et al. 2021) of the PREX-II experiment can be reconciled by an appropriate choice of the parameters. Indeed, this could be accomplished by nucleonic EoS that trade stiffness at high density for softness at low density, e.g.,  $L_{\text{sym}} \lesssim 85$  MeV for  $Q_{\text{sat}} \sim -500$  MeV and  $L_{\text{sym}} \lesssim 45$  MeV (which is at the lower end of the 90% CI of Reed et al. (2021)) for  $Q_{\text{sat}} \sim 900$  MeV. Thus, we conclude that the nucleonic models are not inconsistent with the current information available from multimessenger astrophysics if fairly low values of  $L_{\text{sym}}$  are adopted. We next explore how this situation changes when sequential first-order phase transitions are allowed.

## 2.2. Quark matter equation of state

We will model below the EoS of the quark phase using a *synthetic* constant-sound-speed (CSS) parameterization (Zdunik & Haensel 2013; Alford et al. 2013), which matches well with the predictions based on the NJL model computations that include vector repulsion (e.g., Blaschke et al. 2010; Bonanno & Sedrakian 2012; Klähn et al. 2013). The extension of the CSS EoS to the case of two sequential phase transitions is given by (Alford & Sedrakian 2017),

$$p(\varepsilon) = \begin{cases} p_1, & \varepsilon_1 < \varepsilon < \varepsilon_1 + \Delta\varepsilon_1 \\ p_1 + s_1[\varepsilon - (\varepsilon_1 + \Delta\varepsilon_1)], & \varepsilon_1 + \Delta\varepsilon_1 < \varepsilon < \varepsilon_2 \\ p_2, & \varepsilon_2 < \varepsilon < \varepsilon_2 + \Delta\varepsilon_2 \\ p_2 + s_2[\varepsilon - (\varepsilon_2 + \Delta\varepsilon_2)], & \varepsilon > \varepsilon_2 + \Delta\varepsilon_2 \end{cases} \quad (2)$$

where  $p_{1,2}$  and  $\varepsilon_{1,2}$  are the pressure and energy density at which the transition from hadronic to quark matter and from low-density quark phase (hereafter Q1) to high-density quark phase (hereafter Q2) takes place. We recall that the last phase transition within the quark phase could be the transition between the 2SC to CFL phases, but other options are not excluded. Finally,  $s_1$  and  $s_2$  are squared sound speeds in phases Q1 and Q2, which we quote below in units of the speed of light.

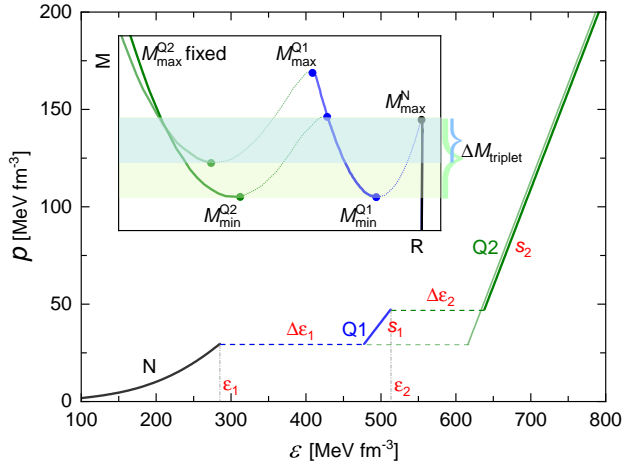


**Figure 2.** Illustrative EoS and  $M$ - $R$  relation for hybrid models. Schematic plot showing the parameterizations of the EoS with single (light green) and double (dark green) phase transitions that could predict the same maximum mass in the quark branch. The emergence of triplet configurations that are characterized by the minimal or maximum masses in each branch is shown in the inset, with one example that obeys conditions (4) and one that does not.

Figure 2 provides a schematic picture of the double phase transition according to equation (2). The six independent parameters which enter Equation (2) are

$$\varepsilon_1, \Delta\varepsilon_1, \varepsilon_2, \Delta\varepsilon_2, s_1, s_2. \quad (3)$$

For a large enough jump in energy density,  $\Delta\varepsilon_1$ , when the central pressure of a star rises above  $p_1$  and Q1 quark matter appears in the core, the star becomes unstable.<sup>1</sup> However, it is also possible to regain stability at higher central pressures: for a certain range of values of  $\varepsilon_1$ ,  $\Delta\varepsilon_1$  and  $s_1$ , there can be a *second stable branch* or “third family” of CSs. In this case, twin configurations may appear, i.e., two stable CSs may have the same mass but different radii and, consequently, deformabilities. If a second phase transition in the quark phase takes place, then a *third stable branch* (or “fourth family”) of CSs containing Q2 quark matter in the core can arise. In analogy to the above, for suitably chosen parameters, *triplet configurations* can arise (Alford & Sedrakian 2017; Li et al. 2020a), in which case there are three stable CSs all having the same masses but different radii as well as deformabilities.

For the convenience of subsequent discussion, let us define the maximal masses of the purely hadronic star (“N star”), the star with a Q1 core (“Q1 star”), and the star with a Q2 inner core and Q1 outer core (“Q2 star”), as

$$M_{\max}^N, M_{\max}^{Q1}, M_{\max}^{Q2}.$$

<sup>1</sup> Here and below we use the standard stability criterion, which implies that CSs are unstable on the descending branch of  $M$ - $R$  diagram and stable on the ascending one. This is not always the case for some boundary conditions on the interface between quark and nuclear matter (see, e.g., Pereira et al. 2018; Gonçalves & Lazzari 2022; Rau & Sedrakian 2022).

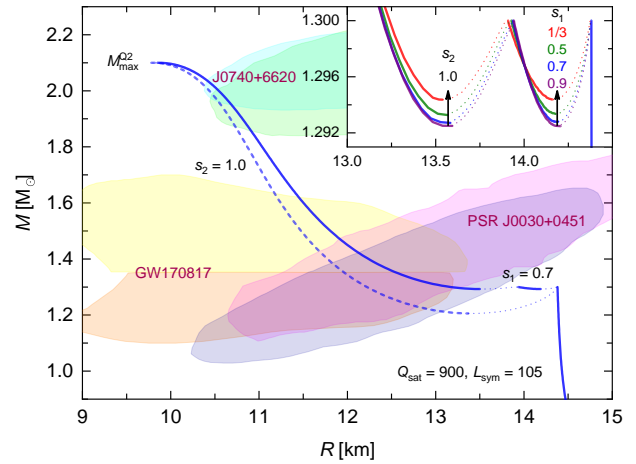


**Figure 3.**  $M$ - $R$  relations showing the stellar sequences have twin or triplet configurations in our setup. The inset illustrates the case with a fixed  $s_2$  value but varying the values of  $s_1$ . For all curves the values of  $s_1, s_2$  are as indicated in the plot. The dotted thin lines indicate unstable configurations.

It is also useful to define the minimum values of the masses of the two stellar branches which consist of stars with only Q1 in the core and with Q1 and Q2 in the core, respectively, as

$$M_{\min}^{Q1}, M_{\min}^{Q2}.$$

See Figure 2 for an illustration of these parameters. We show also in the inset of this figure schematic  $M$ - $R$  relations, which illustrate cases where triplets of stars arise, with each new phase of matter introducing a new family of CSs. The shaded regions in the inset define the range of masses for which triplet configurations arise.

To study the possible role of quark phases in the context of the NICER results for the masses, radii, and GW inferences for the TDs, we reduce the six-dimensional parameter space (3) as follows:

(1) We work in terms of two physical parameters: the maximum mass on the nucleonic branch,  $M_{\max}^N$  (which determines  $\varepsilon_1$ ), and the maximum mass on the hybrid branch,  $M_{\max}^{Q2}$ . (Note that in the case of a single phase transition we adopt the convention of calling the quark phase “Q2”.)

(2) As in Li et al. (2020a), we impose the following conditions (discussed below):

$$M_{\max}^N = M_{\max}^{Q1}, \quad M_{\min}^{Q1} = M_{\min}^{Q2}, \quad M_{\max}^{Q2} \geq M_{\max}^{Q1}. \quad (4)$$

(3) We require the Q2 branch to pass through both the PSR J0740+6620 and J0030+0451 ellipses. This tightly constrains  $s_2$ : we find that its value is highly correlated with  $M_{\max}^{Q2}$ .

(4) We note that the value of  $s_1$  has a negligible influence on the  $M$ - $R$  curve because the Q1 branch is very short.

Using the four constraints/correlations described above, we reduce the six-parameter space (3) to a space with two phys-



ical parameters,  $M_{\max}^N$  and  $M_{\max}^{Q2}$ , which specify a nearly unique  $M$ - $R$  curve.

The conditions (4) ensure that, if in some range of masses twins of the hadronic stars exist due to the phase transition to the Q1 phase, the second phase transition leads to triplets in the *same range* of masses; see the inset of Figure 2 for an illustration. In this inset, we show one example that obeys conditions (4) and one that does not, where both models have the same values for  $M_{\max}^N$  and  $M_{\max}^{Q2}$ . The inset illustrates the behavior that we typically find: if  $M_{\max}^{Q1}$  rises above  $M_{\max}^N$ , achieved by increasing  $\varepsilon_2$  (namely the width of the Q1 phase) then at fixed  $M_{\max}^{Q2}$  we need to reduce the Q1-Q2 energy-density jump  $\Delta\varepsilon_2$  so that  $M_{\min}^{Q2}$  rises above  $M_{\min}^{Q1}$ , which results in a smaller mass range for triplets.

In conclusion, the constraint (4) helps to ensure that triplets exist over a reasonable range of masses,  $\Delta M_{\text{triplet}}$ , for a hybrid EoS model with given values of  $M_{\max}^N$  and  $M_{\max}^{Q2}$ .

Figure 3 illustrates how transitions to and in quark matter allow a nucleonic EoS that is stiff at low densities to be consistent with astrophysical constraints. In this example, the nucleonic EoS has  $L_{\text{sym}} = 105$  MeV (stiff at low density) and  $Q_{\text{sat}} = 900$  MeV (stiff at high density) and we require  $M_{\max}^{Q2} = 2.1 M_{\odot}$  and  $M_{\max}^N = 1.3 M_{\odot}$ , which corresponds to a first-order transition at  $\rho_{\text{tran}} = 1.89 \rho_{\text{sat}}$ . This creates a hybrid branch that is compatible with the GW170817 and PSR J0740+6620 constraints. As an illustration of the limited role of  $s_1$ , the insert of Figure 3 shows that varying  $s_1$  for a fixed  $s_2$  changes the mass by  $0.001 M_{\odot}$ . Note that when we change  $s_1$ , the parameters  $\Delta\varepsilon_1$ ,  $\varepsilon_2$  and  $\Delta\varepsilon_2$  have to be accordingly adjusted, in order to fulfill the first two conditions in Equation (4).

### 3. EXISTENCE OF TWIN OR TRIPLET CONFIGURATIONS

To assess the existence of twin/triplet configurations, we construct EoS from the parameter space of our model that allow for mass twins or triplets that are consistent with both NICER and GW measurements. Specifically, they yield radii that are just above the 90% CI lower limit for PSR J0740+6620 from NICER, and just below the 90% CI upper limit on the radius of a  $1.36 M_{\odot}$  star.<sup>2</sup> In Section 3.1 we will study the stiffer ones that require a transition to quark matter if they are to obey the GW170817 constraint, and in Sections 3.2 and 3.3 we will move on the softer EoS that do not require such a transition.

#### 3.1. Hybrid equation of state featuring sub-canonical-mass twins or triplets

Nucleonic EoS models that are stiff at low and high density (with large  $L_{\text{sym}}$ , in the 100 MeV range, as suggested by Reed et al. (2021)), and positive values of  $Q_{\text{sat}}$  predict a large radius for a canonical-mass CS that is in tension with the GW170817 inference; see Figure 1. We can resolve this

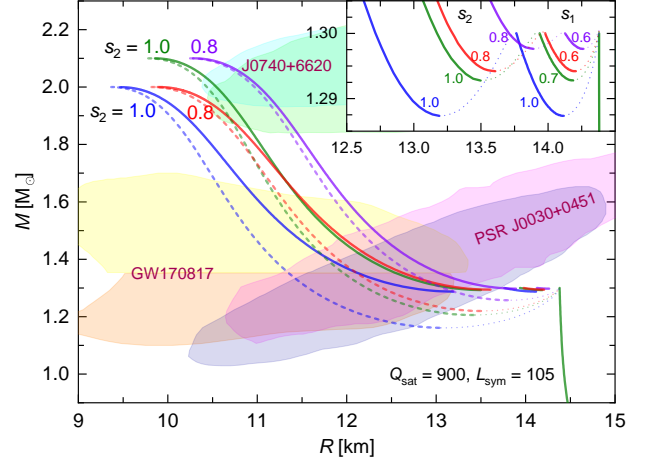


**Figure 4.** Illustrative  $M$ - $R$  relations for hybrid EoS models with stiff nucleonic EoS with single (dashed lines) or double (solid lines) phase translations at subcanonical masses of star sequences. We use nucleonic EoS (with  $Q_{\text{sat}} = 900$ ,  $L_{\text{sym}} = 105$  MeV) and fix  $M_{\max}^N = 1.3 M_{\odot}$  and  $M_{\max}^{Q2} = 2.0, 2.1 M_{\odot}$ . The emergence of subcanonical-mass triplet configurations is shown in the inset. For all the hybrid branches, the values of  $s_1, s_2$  are as indicated in the plot.

by positing a first-order phase transition at low density (i.e., in the hadronic branch ends below a mass of  $1.4 M_{\odot}$ ) leading to a hybrid branch of more compact stars. It should be mentioned that the same effect can be achieved in the EoS models where heavy baryons like  $\Delta$  resonances appear early. This leads to softening of the EoS at intermediate densities, reducing the radius and TD of the star (see, e.g., Li et al. 2020a; Sedrakian et al. 2021, and references therein).

We have shown previously (Li et al. 2021b) that twin configurations can be expected in the mass interval of  $1.2$ - $1.4 M_{\odot}$ . Having this in mind, we fix  $M_{\max}^N = 1.3 M_{\odot}$ , which corresponds to  $\rho_{\text{tran}} \approx 2 \rho_{\text{sat}}$ , and study the general characteristics of the resulting subcanonical-mass twins or triplets.

Figure 4 shows exploratory examples based on the stiffest nucleonic EoS in our collection with  $Q_{\text{sat}} = 900$ ,  $L_{\text{sym}} = 105$  MeV. We show  $M$ - $R$  curves with two values for the maximum mass on the Q2 branch,  $M_{\max}^{Q2} = 2.0$  and  $2.1 M_{\odot}$ , and explore several values of  $s_1$  and  $s_2$ . It is seen that the NICER result for PSR J0740+6620 puts a strong constraint on  $M_{\max}^{Q2}$  and  $s_2$ . For  $M_{\max}^{Q2} = 2.1 M_{\odot}$  it requires  $s_2 \approx 1.0$  and for  $M_{\max}^{Q2} = 2.0 M_{\odot}$  it requires  $s_2 \approx 0.7$ . The resultant hybrid stars are also compatible with the constraints from GW170817 and the NICER results for PSR J0030+0451.

Figure 5 summarizes the mass ranges of twins,  $\Delta M_{\text{twin}}$ , and triplets,  $\Delta M_{\text{triplet}}$ , defined as the range between the maximum value of the nucleonic star mass,  $M_{\max}^N$ , and the common minimum mass of the hybrid star branches,  $M_{\min}^{Q1} = M_{\min}^{Q2}$ . It also gives the difference in the radius,  $\Delta R_{1,3}$ , and TD,  $\Delta \Lambda_{1,3}$ , for stars with mass  $M = 1.3 M_{\odot}$ , as functions of the parameters defining the hybrid EoS model.

<sup>2</sup> Note that  $1.36 M_{\odot}$  is the mass value inferred for an equal-mass binary in the GW170817 event.

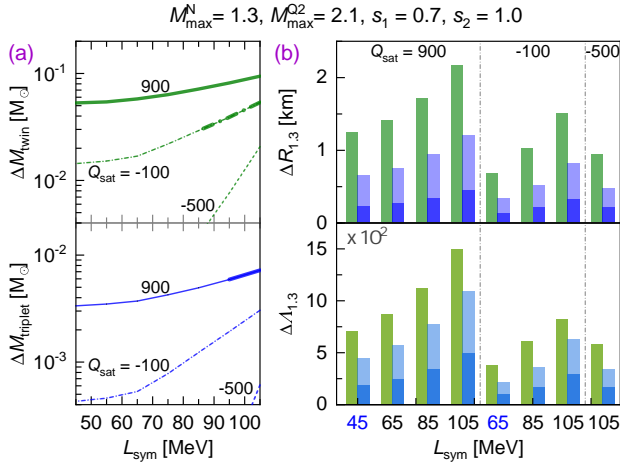


**Figure 5.** Ranges of parameters characterizing twin and triplet configurations for hybrid EoS models. Panel (a) shows the mass ranges of twins  $\Delta M_{\text{twin}}$  and triplet  $\Delta M_{\text{triplet}}$ ; panel (b) shows the difference in the radius  $\Delta R_{1,3}$ , and TD  $\Delta \Lambda_{1,3}$  for twins (in green) and triplets (in blue) with mass  $M = 1.3 M_{\odot}$ , as functions of the parameters of the nucleonic EoS. In panel (a) those models with  $\Delta R_{1,3} \geq 1.0$  km for Q2-N pairs of stars are marked by bold lines. In panel (b), for triplets, the column height shows the value for Q2-N pair of stars, while the values for Q2-Q1 and Q1-N pairs can be read off by the lighter and darker colored column segments, respectively. The colored numbers on the x-axis mark those nucleonic models that meet GW170817’s inference.

From Figures 4 and 5, we observe the systematic features that were established in the case of only twin stars in Li et al. (2021b).

First, increasing  $M_{\text{max}}^{\text{Q2}}$  at fixed  $s_2$  or decreasing  $s_2$  at fixed  $M_{\text{max}}^{\text{Q2}}$  tends to reduce the mass range of triplets and twins. At the same time, the instability region of mass (or radius) between nucleonic and hybrid stars decreases as the value of  $M_{\text{max}}^{\text{Q2}}$  increases at fixed  $s_2$ , or as  $s_2$  decreases at fixed  $M_{\text{max}}^{\text{Q2}}$ . A smaller value of  $s_2$ , in the current setup, allows a smaller  $\Delta \varepsilon_2$  and for a resulting steep decrease in the mass range for twins and/or triplets. For our parameter choice, in order for the  $M$ - $R$  curves to pass through the NICER 90% CI region for PSR J0740+6620, it requires  $s_2$  close to 1.0.

Second, for stiffer nucleonic EoS featuring larger values of  $L_{\text{sym}}$  and/or  $Q_{\text{sat}}$ , the range of masses where twin/triplet stars appear is larger. This is because for hybrid EoS with fixed  $M_{\text{max}}^{\text{Q2}}$ , increased stiffness of the nucleonic EoS must be offset by a softer quark phase, e.g., larger energy-density jumps  $\Delta \varepsilon_1$ ,  $\Delta \varepsilon_2$ , or width  $\varepsilon_2 - \varepsilon_1 - \Delta \varepsilon_1$ . This makes the hybrid branch more compact while the stiffer nucleonic EoS makes the hadronic branch less compact, i.e., the difference in radius is larger. The mass ranges of triplet stars  $\Delta M_{\text{triplet}}$  are typically  $\sim 10^{-3} M_{\odot}$ , which is one order smaller than the mass range for twin stars,  $\Delta M_{\text{twin}}$ .

Third, the differences in radii and deformabilities for triplet stars are typically 40-50% smaller than for twin stars. The values of  $\Delta R_{1,3}$  for N-Q2 pairs are, at most, about 1.0 km;

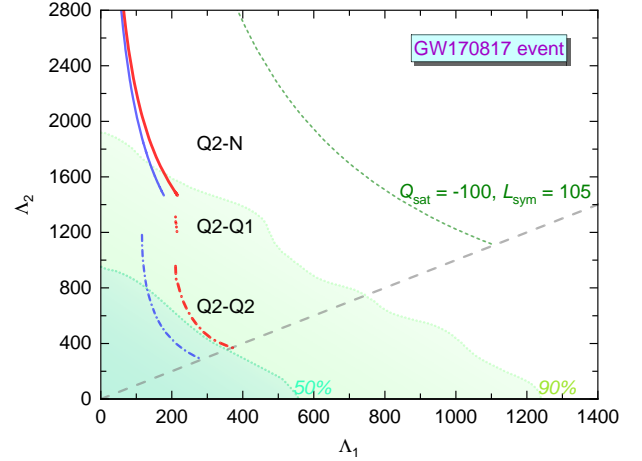


**Figure 6.** TDs of compact objects with single (in blue) and double (in red) phase transitions for a fixed value of binary chirp mass  $\mathcal{M} = 1.186 M_{\odot}$  inferred from the GW170817 event, varying the mass ratio. The hybrid models are constructed from nucleonic EoS by setting  $M_{\text{max}}^{\text{N}} = 1.3 M_{\odot}$  of the hadronic branch,  $M_{\text{max}}^{\text{Q1}} = 1.3 M_{\odot}$ ,  $s_1 = 0.7$  of the Q1 branch, and  $M_{\text{max}}^{\text{Q2}} = 2.1 M_{\odot}$ ,  $s_2 = 1.0$  of the Q2 branch. For models with mass twins, the two types of pairs for stars with masses  $M_1$  and  $M_2$  are Q2-N and Q2-Q1, while for models with mass triplets the three types of pairs are Q2-N, Q2-Q1, and Q2-Q2. The shaded regions correspond to the 50% and 90% CIs taken from the analysis of GW170817 within the PhenomPNRT model (Abbott et al. 2018).

the values for N-Q1 or Q1-Q2 pairs are even smaller. Directly observing twins or triplets would therefore require a radius measurement accuracy of better than 1 km. This corresponds to a radius measurement accuracy of less than 10%, which is not yet available, but NICER aims to achieve 5% accuracy in the future.<sup>3</sup> The difference in the TDs of triplets  $\Delta \Lambda_{1,3}$  can be several hundred to one thousand, so, given TD measurements with error bars in the few hundred range, there is a possibility that TD measurements from the inspiral phase of CS mergers could identify triplets.

We now compare our theoretical TDs for hybrid star models with the observational constraints for this quantity obtained from the analysis of the GW170817 event (Abbott et al. 2018). We take the chirp mass as  $\mathcal{M} = 1.186 M_{\odot}$  inferred from this merger and carry out the comparison only using the analysis which assumes the (more plausible) low-spin case (Abbott et al. 2018). For this binary, the component masses are found to be in the range 1.16-1.60  $M_{\odot}$  at 90% CI. In the scenarios that we are exploring in this section, this implies that at least one of the components should be a hybrid star.

Figure 6 displays the TDs  $\Lambda_1$  and  $\Lambda_2$  of the stars involved in the binary with masses  $M_1$  (the primary, which is defined as the heavier of the pair) and  $M_2$  (secondary) in the cases

<sup>3</sup> NICER Home: <https://heasarc.gsfc.nasa.gov/docs/nicer/>

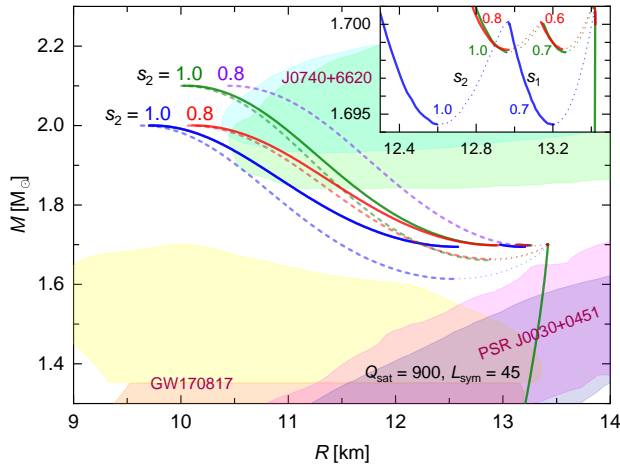


**Figure 7.** Same as in Figure 4, but for hybrid EoS models with an intermediate-soft nucleonic EoS that allows single (dashed lines) or double (solid lines) phase transitions to appear in high-mass stars. The results are constructed from a nucleonic EoS ( $Q_{\text{sat}} = 900, L_{\text{sym}} = 45$  MeV) by fixing  $M_{\text{max}}^N/M_{\odot} = 1.7$  of the nucleonic branch, while varying the maximum mass  $M_{\text{max}}^{Q2}/M_{\odot} = 2.0, 2.1$  of the Q2 branch.

of single and double phase transitions. We show curves for two models, one with a single Q2 phase and one with both Q1 and Q2 phases. The models are constructed from soft-stiff nucleonic EoS ( $Q_{\text{sat}} = -100$  and  $L_{\text{sym}} = 105$  MeV) by setting  $M_{\text{max}}^N = 1.3 M_{\odot}$  of the hadronic branch, and combined quark EoS featuring  $M_{\text{max}}^{Q1} = 1.3 M_{\odot}$ ,  $s_1 = 0.7$  of the Q1 branch, and  $M_{\text{max}}^{Q2} = 2.1 M_{\odot}$ ,  $s_2 = 1.0$  of the Q2 branch. The diagonal line corresponds to the case of an equal-mass binary with  $M_{1,2} = 1.362 M_{\odot}$ . The shaded areas correspond to the 90% and 50% CIs, which are inferred from the analysis of the GW170817 event using the PhenomPNRT waveform model (Abbott et al. 2019).

The hypothesis of a stiff nucleonic EoS with a low-density transition to quark matter is compatible with limits on the TD from GW170817. In Figure 6 we show how this is possible: for the EoS models plotted there, both stars in the GW170817 merger could be hybrid, either Q2-Q1 or Q2-Q2, or one could be a heavy hybrid star and the other could be a nucleonic star near the top of the nucleonic branch.

### 3.2. Hybrid equation of state featuring high-mass twins or triplets

Consider next a class of less stiff nucleonic EoS models that could (approximately) match GW170817's inference without a phase transition to quark matter. Figure 7 shows examples of the nucleonic EoS with  $Q_{\text{sat}} = 900, L_{\text{sym}} = 45$  MeV for a fixed value of  $M_{\text{max}}^N = 1.70 M_{\odot}$ , which corresponds to  $\rho_{\text{tran}} = 2.41 \rho_{\text{sat}}$ . The values of the remaining parameters — the sound speed squares,  $s_1$  and  $s_2$ , and the maximum mass,  $M_{\text{max}}^{Q2}$  — are chosen such that the Q2 branch is located close to the lower bound of the NICER's 90% CI for the radius of PSR J0740+6620. Within this setup, we find

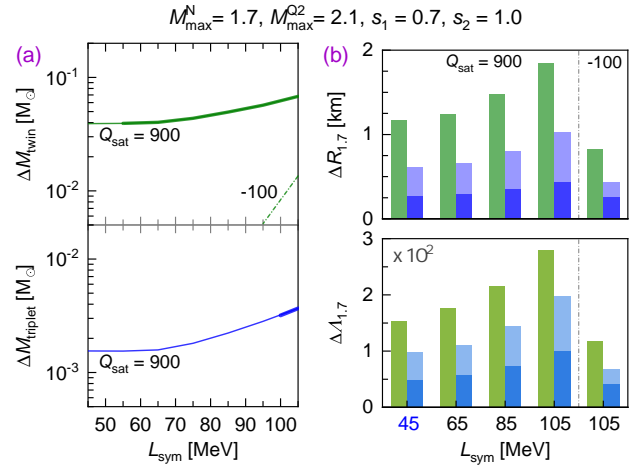


**Figure 8.** Same as in Figure 5, but for hybrid EoS models with  $M_{\text{max}}^N/M_{\odot} = 1.7$ . In panel (a) those models with  $\Delta R_{1.7} \geq 1.0$  km for Q2-N pairs of stars are marked by bold lines. Notice that there are almost no twin/triplet configurations for a nucleonic EoS models with  $Q_{\text{sat}} = -500$  and  $-100$  MeV.

the acceptable models are those which have the values of the two parameters  $M_{\text{max}}^{Q2}/M_{\odot}$  and  $s_2$  defined as pairs,  $(2.1, 1.0)$  or  $(2.0, 0.8)$ , which cover the approximate mass ranges for twins and triplets.

In Figure 8 we show the ranges of parameters characterizing twin and triplet configurations by varying continuously  $L_{\text{sym}}$  for some fixed values of  $Q_{\text{sat}}$ . Note that this figure includes for completeness also the results for stiff nucleonic EoS that predict a  $M$ - $R$  range outside of the GW170817 ellipses.

The general features found for the case of hybrid models featuring subcanonical-mass twin/triplet configurations above are replicated within this class as well. However, we find (almost) no twin/triplet solutions for nucleonic models with  $Q_{\text{sat}} = -500$ , and  $-100$  MeV; see Figure 8(a). This implies that the appearance of intermediate-mass twin/triplet configurations requires a nucleonic EoS which is stiff in the entire relevant range, so that the radius of a  $1.7 M_{\odot}$  star  $R_{1.7} \gtrsim 13.5$  km. However, such nucleonic EoS all predict  $R_{1.4} \gtrsim 13.2$  km which is inconsistent with GW170817's constraint. As a result, the few valid hybrid EoS models in our collection are those constructed from nucleonic EoS with  $Q_{\text{sat}} \sim 900$  and  $L_{\text{sym}} \sim 45$  MeV. Although we find twin/triplet configurations, as seen in Figure 8(b), the differences in their radii ( $\Delta R \lesssim 1$  km) and TDs ( $\Delta \Lambda \lesssim 100$ ) are beyond current detection capability.

We now turn to the possible constraints placed by the TDs on our collection of hybrid EoS models. To this end, we set the chirp mass  $\mathcal{M} = 1.44 M_{\odot}$  inferred from the GW190425 event (Abbott et al. 2020a). For this binary, the 90% CIs for the component masses range from  $1.46$  to  $1.87 M_{\odot}$  if we restrict a low-spin prior (Abbott et al. 2020a). The GW190425 observational analysis, however, does not provide significantly novel information on the stellar matter EoS (Abbott et al. 2020a). For instance, the estimation of the combined

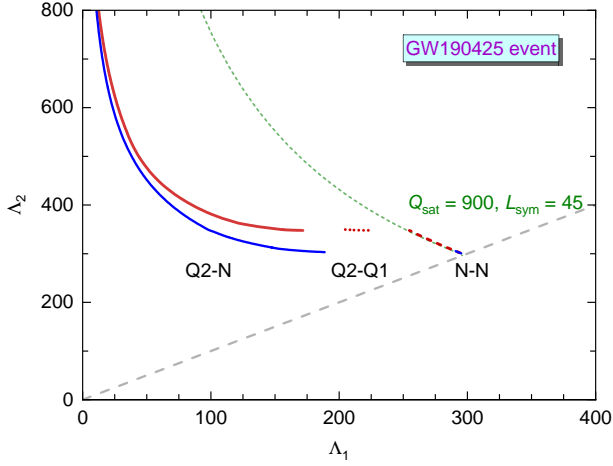


**Figure 9.** TDs of compact objects with single (in blue) and double phase (in red) transitions for a fixed value of binary chirp mass  $\mathcal{M} = 1.44 M_\odot$  inferred from the GW190425 event (Abbott et al. 2020a). The hybrid EoS models are constructed from a nucleonic model with  $M_{\text{max}}^{\text{N}} = 1.7 M_\odot$  of the hadronic branch,  $M_{\text{max}}^{\text{Q1}} = 1.7 M_\odot$ ,  $s_1 = 0.7$  of the Q1 branch, and  $M_{\text{max}}^{\text{Q2}} = 2.1 M_\odot$ ,  $s_2 = 1.0$  of the Q2 branch. For models with mass twins, the two types of pairs for stars with masses  $M_1$  and  $M_2$  are Q2-N and N-N, while for models with mass triplet the three types of pairs are Q2-N, Q2-Q1, and N-N.

dimensionless TD  $\tilde{\Lambda}_{1.44} \lesssim 600$ , which could be converted to  $\Lambda_{1.654} \lesssim 600$  for a star with mass  $M = 1.654 M_\odot$ . This upper limit is consistent with the values of TDs predicted by our stiffest nucleonic EoS ( $Q_{\text{sat}} = 900, L_{\text{sym}} = 105$  MeV); see Figure 1 where the values of TDs are quoted.

Figure 9 displays the TDs  $\Lambda_1$  and  $\Lambda_2$  of the stars involved in a binary with masses  $M_1$  and  $M_2$  in the cases of single and double phase transitions for a selection of hybrid EoS. The models are constructed from stiff-soft EoS with  $Q_{\text{sat}} = 900$  and  $L_{\text{sym}} = 45$  MeV by setting  $M_{\text{max}}^{\text{N}} = 1.7 M_\odot$ ,  $M_{\text{max}}^{\text{Q1}} = 1.7 M_\odot$ ,  $s_1 = 0.7$  and  $M_{\text{max}}^{\text{Q2}} = 2.1 M_\odot$ ,  $s_2 = 1.0$ . Let us recall that in the case of a single phase transition it is assumed that the transition takes place directly from the hadronic phase to the Q2 quark phase. The diagonal line corresponds to the case of an equal-mass binary with  $M_{1,2} = 1.654 M_\odot$ . In this case the maximum mass of the nucleonic branch of the sequence  $M_{\text{max}}^{\text{N}} = 1.70 M_\odot$  is slightly higher than the value of the equal-mass case  $1.654 M_\odot$  (Abbott et al. 2020a). The possible types of pairs differ from previous results in Figure 6. In general, two types of pairs of CSs could be involved in such a merger event, namely Q2-N and N-N for EoS models with a single phase transition featuring mass twins; and three types of pairs of CSs, namely Q2-N, Q2-Q1, and N-N for EoS models with two sequential phase transitions featuring triplets. As far as observations are concerned, we note that the difference in the TDs of triplets  $\Delta\Lambda_{1.7}$  for N-Q2 pairs is, at most,  $\sim 100$ . This makes it challenging to distinguish between nucleonic and hybrid stars by analyzing the TDs.

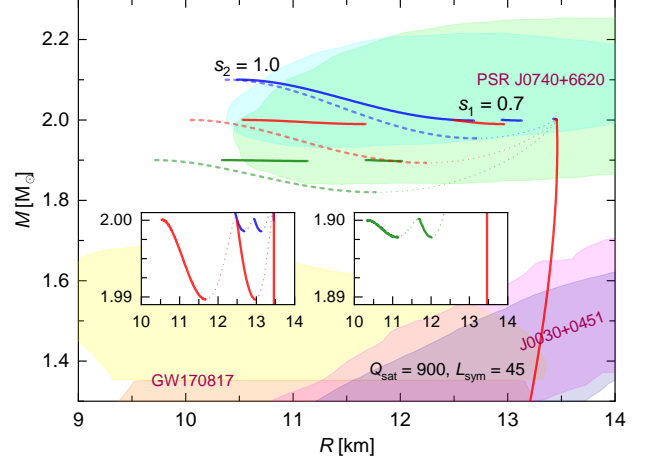


**Figure 10.** Same as in Figure 4, but for hybrid EoS models with an intermediate-soft nucleonic EoS that allows single (dashed lines) or double (solid lines) phase transitions to appear in high-mass stars. The results are constructed from a nucleonic EoS ( $Q_{\text{sat}} = 900, L_{\text{sym}} = 45$  MeV) by fixing  $M_{\text{max}}^{\text{N}}/M_\odot = 2.0$  of the nucleonic branch, while varying the maximum mass  $M_{\text{max}}^{\text{Q2}}/M_\odot = 1.9, 2.0, \text{ and } 2.1$  of the Q2 branch.

### 3.3. Hybrid equation of state featuring massive twins or triplets

Finally, we consider an extreme class of models where the phase transitions occur at high densities  $\rho_{\text{tran}} \sim 3.0 \rho_{\text{sat}}$ , i.e., a strong phase transition takes place in CSs of the nucleonic branch with a mass close to the value  $\sim 2.0 M_\odot$  of observed massive pulsars. In this case, NICER's 90% CI for PSR J0740+6620 does not provide significant constraints on the possibility of phase transitions. This is because the maximum mass of the nucleonic sequence satisfies the requirements set by the NICER measurement and any hybrid branches of CSs are allowed to exist even outside the 90% CI region.

Figure 10 shows model EoS for fixed  $Q_{\text{sat}} = 900, L_{\text{sym}} = 45$  MeV,  $M_{\text{max}}^{\text{N}}/M_\odot = 2.0$  (which corresponds to  $\rho_{\text{tran}} = 2.76 \rho_{\text{sat}}$ ), and  $(s_1, s_2) = (0.7, 1.0)$  for values of  $M_{\text{max}}^{\text{Q2}}/M_\odot = 1.9, 2.0, \text{ and } 2.1$ . For the model with  $M_{\text{max}}^{\text{Q2}}/M_\odot = 1.9$ , i.e., a case of  $M_{\text{max}}^{\text{Q2}} < M_{\text{max}}^{\text{N}}$ , we drop the first condition in Equation (4) and use instead  $M_{\text{max}}^{\text{Q2}} = M_{\text{max}}^{\text{Q1}}$ . It is seen from the insets of Figure 10 that the most pronounced mass twins and/or mass triplets appear in the sequences when  $M_{\text{max}}^{\text{Q2}}/M_\odot \approx 2.0$ . Figure 11 gives the ranges of parameters that characterize twin and triplet configurations as a function of the model parameters defining the EoS. In this class, again, we find no twin/triplet solutions for models with  $Q_{\text{sat}} = -500$  MeV.

From Figures 10 and 11 (a) we conclude that the range of masses containing twin/triplet configurations (if they are allowed by the parameters of the nucleonic EoS) is somewhat extended compared to the  $M_{\text{max}}^{\text{N}}/M_\odot = 1.3$  and  $1.7$  cases discussed in previous subsections. The values of  $\Delta M_{\text{twin}}$  could be as large as  $0.1 M_\odot$ , which is in principle within the accuracy of mass measurements via the relativistic Shapiro time delay. The radius difference between the radii of twins,



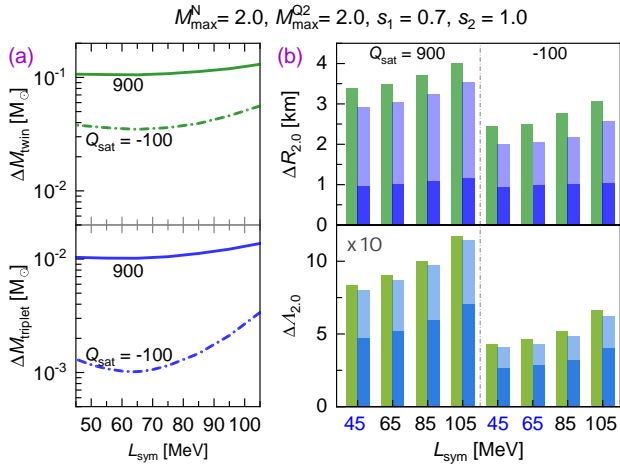


**Figure 11.** Same as in Figure 5, but for hybrid EoS models with  $M_{\text{max}}^{\text{N}}/M_\odot = 2.0$ . Notice that no twin/triplet configurations were found for nucleonic EoS models with  $Q_{\text{sat}} = -500$  MeV.

$\Delta R_{\text{twin}}$ , can reach up to 2-3 km, which is again within the accuracy that is achieved routinely in NICER data analysis. However, in the case of triplet configurations, the values of  $\Delta M_{\text{triplet}}$  are, at most,  $0.01 M_\odot$ , which is beyond the current detection capability. The radius difference of triplets,  $\Delta R_{\text{triplet}}$ , can be as large as 1 km for Q1-N or Q1-Q2 pairs, and 2 km for N-Q2 pairs; see Figure 11 (b). The differences in the TDs of twins and triplets  $\Delta \Lambda_{2,0}$ , as expected, are only several tens; see Figure 11 (b). This implies that TD measurements are not useful for distinguishing very massive nucleonic stars from their hybrid twins. We recall that we consider only the class of hybrid EoS models for which the nucleonic EoS satisfies the GW170817 constraints.

### 3.4. Remarks

Let us close this section with some general remarks. Combining the results presented above, it can be concluded that (i) if the nucleonic EoS is stiff (i.e., there is tension with GW170817’s inference) and multiple stable branches with twin or triplet configurations exist, then the transition from the nucleonic branch likely happens at a low density,  $\rho_{\text{tran}} \lesssim 2.0 \rho_{\text{sat}}$ , with a corresponding mass  $M_{\text{max}}^{\text{N}} \lesssim 1.3$ - $1.4 M_\odot$ ; and (ii) for a soft nucleonic EoS, which is consistent with GW170817’s inference, the transition density could be higher,  $\rho_{\text{tran}} \sim 3.0 \rho_{\text{sat}}$ , with a corresponding mass  $M_{\text{max}}^{\text{N}} \sim 2.0 M_\odot$ .

We found narrow ranges of masses and a modest radius difference for low-mass and intermediate-mass twins/triplets, which are a consequence of the constraint imposed by the large radius of PSR J0740+6620. It limits the allowed range of the reduction of the radius of a hybrid star and makes it challenging to distinguish between nucleonic and hybrid stars. The situation is more optimistic if the nucleonic branch reaches the maximum value  $\sim 2.0 M_\odot$ . Finally, note that in all the above discussed models, a larger mass range for twin/triplet configurations exists for models that have a large value of sound-speed square  $s_2 \leq 1$ .

## 4. CONCLUSIONS

In this paper, we extended our analysis (Li et al. 2021b) of the two recent observational/experimental results — the inference of the radius of PSR J0740+6620 (Riley et al. 2021; Miller et al. 2021) and the neutron skin thickness by analysis of the PREX-II experiment (Reed et al. 2021; Reinhard et al. 2021) — to a broader class of models. These now include (i) double phase transitions in the quark phase and (ii) transition to quark matter at low, intermediate, and high densities. In doing so, we continued using a density-functional approach to nucleonic matter which is calibrated to nuclear phenomenology, and the CSS parameterization to describe high-density quark matter.

We have assessed the existence of twin or triplet configurations for three classes of nucleonic stars. For the class where nucleonic EoS models predict a large radius for a canonical-mass ( $M = 1.4 M_\odot$ ) star, we show that the tension between GW170817’s inference for the radius and models with large values of  $L_{\text{sym}}$  can be mitigated (if not completely removed) by a low-density phase transition to quark matter and the formation of low-mass hybrid stars. This leads always to the appearance of twins and/or triplets, in the cases of single and double phase transitions, respectively. For the class of less stiff nucleonic EoS models that are consistent with GW170817’s inference, we find that for nucleonic branches extending up to  $\sim 1.7 M_\odot$ , twins or triplets only exist in very small mass ranges, i.e.,  $\Delta M_{\text{twin}} \lesssim 0.04 M_\odot$  and  $\Delta M_{\text{triplet}} \lesssim 0.002 M_\odot$ .

If the nucleonic branch extends up to  $\sim 2.0 M_\odot$  (i.e., the radius of PSR J0740+662 can be attributed to the nucleonic branch), twins and triplets can exist in narrow mass ranges  $\Delta M_{\text{twin}} \lesssim 0.1 M_\odot$  for twins and  $\Delta M_{\text{triplet}} \lesssim 0.01 M_\odot$  for triplets. As expected, the ranges of mass and radius (and TD) for the existence of mass twins and mass triplets are larger for the stiff nucleonic EoS model. The largest ranges of twins and triplets are generally supported by models with  $s_{1,2} \leq 1.0$ , which allow for maximum masses  $M_{\text{max}}^{\text{Q2}} \sim 2.1 M_\odot$ . The most pronounced twins and/or triplet configurations are found to appear in sequences with a mass of about  $2.0 M_\odot$ .

We also extended our previous analysis of the TD (Li et al. 2020a, 2021b) to our current models, with a focus on sequences that contain twin and triplet configurations. The resulting TD diagram can be used in future analysis of binary neutron star merger events in a search for signatures of QCD phase transition(s). In particular, we demonstrated that low-mass twins and triplets differ quantitatively by their TDs, while massive twins and triplets differ quantitatively by their radii; see Figures 5 and 11. This highlights the prospects of confirmation of the existence of twin and triplet stars from future measurements similar to those used in our analysis (i.e., X-ray measurements of radii and GW measurements of TDs). Specifically, we expect a significantly smaller radius (by about 1-2 km) for hybrid stars compared to purely nucleonic stars. In merger events, finding stars with similar masses but significantly different values of TD would be a

clear indication of a phase transition. In this case, the TDs will be drawn, respectively, from the disconnected branches in the  $\Lambda$ - $\Lambda$  diagrams, one corresponding to the nucleonic branch and another to the hybrid branch. There are other observables that we have not discussed that can indicate a first-order phase transition. For example, Bauswein et al. (2019) find that the dominant postmerger GW frequency for hybrid and nucleonic stars differ significantly from each other. Furthermore, the gravitational radiation from asymmetric supernova explosions (Fischer 2021; Bauswein et al. 2022) will carry the imprints of separate phase transitions. Also, matter accretion onto a CS will lead to its compression, two successive phase transitions and two separate explosions with energy release associated with them (Zdunik et al. 2008; Abdikamalov et al. 2009; Lin et al. 2011). Finally, we stress once again that the present astrophysical and nuclear physics

data do not prohibit the existence of mass twin and/or mass triplet if strong first-order phase transitions occur in dense matter.

J. L. acknowledges the support of the National Natural Science Foundation of China (Grant No. 12105232), the Fundamental Research Funds for the Central Universities (Grant No. SWU-020021), and by the Venture & Innovation Support Program for Chongqing Overseas Returnees (Grant No. CX2021007). A. S. is supported by the Deutsche Forschungsgemeinschaft Grant No. SE 1836/5-2 and the Polish NCN Grant No. 2020/37/B/ST9/01937 at Wroclaw University. M. A. is supported by the U.S. Department of Energy, Office of Science, Office of Nuclear Physics under Award No. DE-FG02-05ER41375.

## REFERENCES

- Abbott, B. P., Abbott, R., Abbott, T. D., et al. 2017, *PhRvL*, 119, 161101, doi: [10.1103/PhysRevLett.119.161101](https://doi.org/10.1103/PhysRevLett.119.161101)
- Abbott, B. P., Abbott, R., Abbot, T. D., et al. 2018, *PhRvL*, 121, 161101, doi: [10.1103/PhysRevLett.121.161101](https://doi.org/10.1103/PhysRevLett.121.161101)
- . 2019, *PhRvX*, 9, 011001, doi: [10.1103/PhysRevX.9.011001](https://doi.org/10.1103/PhysRevX.9.011001)
- . 2020a, *ApJL*, 892, L3, doi: [10.3847/2041-8213/ab75f5](https://doi.org/10.3847/2041-8213/ab75f5)
- Abbott, R., Abbott, T. D., Abraham, S., et al. 2020b, *ApJL*, 896, L44, doi: [10.3847/2041-8213/ab960f](https://doi.org/10.3847/2041-8213/ab960f)
- Abdikamalov, E. B., Dimmelmeier, H., Rezzolla, L., & Miller, J. C. 2009, *MNRAS*, 392, 52, doi: [10.1111/j.1365-2966.2008.14056.x](https://doi.org/10.1111/j.1365-2966.2008.14056.x)
- Adhikari, D., Albatineh, H., Androic, D., et al. 2021, *PhRvL*, 126, 172502, doi: [10.1103/PhysRevLett.126.172502](https://doi.org/10.1103/PhysRevLett.126.172502)
- Alford, M. G., Han, S., & Prakash, M. 2013, *PhRvD*, 88, 083013, doi: [10.1103/PhysRevD.88.083013](https://doi.org/10.1103/PhysRevD.88.083013)
- Alford, M. G., Rajagopal, K., Reddy, S., & Wilczek, F. 2001, *PhRvD*, 64, 074017, doi: [10.1103/PhysRevD.64.074017](https://doi.org/10.1103/PhysRevD.64.074017)
- Alford, M. G., Schmitt, A., Rajagopal, K., & Schäfer, T. 2008, *RvMP*, 80, 1455, doi: [10.1103/RevModPhys.80.1455](https://doi.org/10.1103/RevModPhys.80.1455)
- Alford, M. G., & Sedrakian, A. 2017, *PhRvL*, 119, 161104, doi: [10.1103/PhysRevLett.119.161104](https://doi.org/10.1103/PhysRevLett.119.161104)
- Alvarez-Castillo, D. E., Blaschke, D. B., Grunfeld, A. G., & Pagura, V. P. 2019, *PhRvD*, 99, 063010, doi: [10.1103/PhysRevD.99.063010](https://doi.org/10.1103/PhysRevD.99.063010)
- Anglani, R., Casalbuoni, R., Ciminale, M., et al. 2014, *RvMP*, 86, 509, doi: [10.1103/RevModPhys.86.509](https://doi.org/10.1103/RevModPhys.86.509)
- Annala, E., Gorda, T., Kurkela, A., & Vuorinen, A. 2018, *PhRvL*, 120, 172703, doi: [10.1103/PhysRevLett.120.172703](https://doi.org/10.1103/PhysRevLett.120.172703)
- Baldo, M., & Burgio, G. F. 2016, *PrPNP*, 91, 203, doi: [10.1016/j.pnpnp.2016.06.006](https://doi.org/10.1016/j.pnpnp.2016.06.006)
- Bauswein, A., Bastian, N.-U. F., Blaschke, D. B., et al. 2019, *PhRvL*, 122, 061102, doi: [10.1103/PhysRevLett.122.061102](https://doi.org/10.1103/PhysRevLett.122.061102)
- Bauswein, A., Blaschke, D., & Fischer, T. 2022, arXiv e-prints, arXiv:2203.17188, doi: [10.48550/arXiv.2203.17188](https://doi.org/10.48550/arXiv.2203.17188)
- Biswas, B. 2022, *ApJ*, 926, 75, doi: [10.3847/1538-4357/ac447b](https://doi.org/10.3847/1538-4357/ac447b)
- Blaschke, D., Klahn, T., Lastowiecki, R., & Sandin, F. 2010, *JPhG*, 37, 094063, doi: [10.1088/0954-3899/37/9/094063](https://doi.org/10.1088/0954-3899/37/9/094063)
- Bonanno, L., & Sedrakian, A. 2012, *A&A*, 539, A16, doi: [10.1051/0004-6361/201117832](https://doi.org/10.1051/0004-6361/201117832)
- Burgio, G. F., Drago, A., Pagliara, G., Schulze, H. J., & Wei, J. B. 2018, *ApJ*, 860, 139, doi: [10.3847/1538-4357/aac6ee](https://doi.org/10.3847/1538-4357/aac6ee)
- Christian, J.-E., & Schaffner-Bielich, J. 2022, *ApJ*, 935, 122, doi: [10.3847/1538-4357/ac75cf](https://doi.org/10.3847/1538-4357/ac75cf)
- Christian, J.-E., Zacchi, A., & Schaffner-Bielich, J. 2019, *PhRvD*, 99, 023009, doi: [10.1103/PhysRevD.99.023009](https://doi.org/10.1103/PhysRevD.99.023009)
- Collins, J. C., & Perry, M. J. 1975, *PhRvL*, 34, 1353, doi: [10.1103/PhysRevLett.34.1353](https://doi.org/10.1103/PhysRevLett.34.1353)
- Contrera, G. A., Blaschke, D., Carlomagno, J. P., Grunfeld, A. G., & Liebing, S. 2022, *PhRvC*, 105, 045808, doi: [10.1103/PhysRevC.105.045808](https://doi.org/10.1103/PhysRevC.105.045808)
- Cromartie, H. T., Fonseca, E., Ransom, S. M., et al. 2020, *NatAs*, 4, 72, doi: [10.1038/s41550-019-0880-2](https://doi.org/10.1038/s41550-019-0880-2)
- Danielewicz, P., & Lee, J. 2014, *NuPhA*, 922, 1, doi: [10.1016/j.nuclphysa.2013.11.005](https://doi.org/10.1016/j.nuclphysa.2013.11.005)
- Drischler, C., Han, S., & Reddy, S. 2022, *PhRvC*, 105, 035808, doi: [10.1103/PhysRevC.105.035808](https://doi.org/10.1103/PhysRevC.105.035808)
- Essick, R., Landry, P., & Holz, D. E. 2020, *PhRvD*, 101, 063007, doi: [10.1103/PhysRevD.101.063007](https://doi.org/10.1103/PhysRevD.101.063007)
- Essick, R., Tews, I., Landry, P., & Schwenk, A. 2021, *PhRvL*, 127, 192701, doi: [10.1103/PhysRevLett.127.192701](https://doi.org/10.1103/PhysRevLett.127.192701)
- Fattoyev, F. J., Horowitz, C. J., Piekarewicz, J., & Reed, B. 2020, *PhRvC*, 102, 065805, doi: [10.1103/PhysRevC.102.065805](https://doi.org/10.1103/PhysRevC.102.065805)
- Fischer, T. 2021, *EPJA*, 57, 270, doi: [10.1140/epja/s10050-021-00571-z](https://doi.org/10.1140/epja/s10050-021-00571-z)

- Fonseca, E., Cromartie, H. T., Pennucci, T. T., et al. 2021, *ApJL*, 915, L12, doi: [10.3847/2041-8213/ac03b8](https://doi.org/10.3847/2041-8213/ac03b8)
- Gonçalves, V. P., & Lazzari, L. 2022, *EPJC*, 82, 288, doi: [10.1140/epjc/s10052-022-10273-5](https://doi.org/10.1140/epjc/s10052-022-10273-5)
- Huth, S., Pang, P. T. H., Tews, I., et al. 2022, *Nature*, 606, 276, doi: [10.1038/s41586-022-04750-w](https://doi.org/10.1038/s41586-022-04750-w)
- Itoh, N. 1970, *PTPh*, 44, 291, doi: [10.1143/PTP.44.291](https://doi.org/10.1143/PTP.44.291)
- Ivanenko, D. D., & Kurdgelaidze, D. F. 1965, *Astrophysics*, 1, 251, doi: [10.1007/BF01042830](https://doi.org/10.1007/BF01042830)
- Jokela, N., Järvinen, M., & Remes, J. 2022, *PhRvD*, 105, 086005, doi: [10.1103/PhysRevD.105.086005](https://doi.org/10.1103/PhysRevD.105.086005)
- Khadkikar, S., Raduta, A. R., Oertel, M., & Sedrakian, A. 2021, *PhRvC*, 103, 055811, doi: [10.1103/PhysRevC.103.055811](https://doi.org/10.1103/PhysRevC.103.055811)
- Klähn, T., Łastowiecki, R., & Blaschke, D. 2013, *PhRvD*, 88, 085001, doi: [10.1103/PhysRevD.88.085001](https://doi.org/10.1103/PhysRevD.88.085001)
- Lalazissis, G. A., Niksic, T., Vretenar, D., & Ring, P. 2005, *PhRvC*, 71, 024312, doi: [10.1103/PhysRevC.71.024312](https://doi.org/10.1103/PhysRevC.71.024312)
- Lattimer, J. M., & Lim, Y. 2013, *ApJ*, 771, 51, doi: [10.1088/0004-637X/771/1/51](https://doi.org/10.1088/0004-637X/771/1/51)
- Legred, I., Chatziioannou, K., Essick, R., Han, S., & Landry, P. 2021, *PhRvD*, 104, 063003, doi: [10.1103/PhysRevD.104.063003](https://doi.org/10.1103/PhysRevD.104.063003)
- Li, A., Miao, Z., Han, S., & Zhang, B. 2021a, *ApJ*, 913, 27, doi: [10.3847/1538-4357/abf355](https://doi.org/10.3847/1538-4357/abf355)
- Li, J. J., & Sedrakian, A. 2019, *PhRvC*, 100, 015809, doi: [10.1103/PhysRevC.100.015809](https://doi.org/10.1103/PhysRevC.100.015809)
- Li, J. J., Sedrakian, A., & Alford, M. 2020a, *PhRvD*, 101, 063022, doi: [10.1103/PhysRevD.101.063022](https://doi.org/10.1103/PhysRevD.101.063022)
- . 2021b, *PhRvD*, 104, L121302, doi: [10.1103/PhysRevD.104.L121302](https://doi.org/10.1103/PhysRevD.104.L121302)
- Li, J. J., Sedrakian, A., & Weber, F. 2020b, *PhLB*, 810, 135812, doi: [10.1016/j.physletb.2020.135812](https://doi.org/10.1016/j.physletb.2020.135812)
- Lin, W., Li, B.-A., Xu, J., Ko, C. M., & Wen, D. H. 2011, *PhRvC*, 83, 045802, doi: [10.1103/PhysRevC.83.045802](https://doi.org/10.1103/PhysRevC.83.045802)
- Malfatti, G., Orsaria, M. G., Ranea-Sandoval, I. F., Contrera, G. A., & Weber, F. 2020, *PhRvD*, 102, 063008, doi: [10.1103/PhysRevD.102.063008](https://doi.org/10.1103/PhysRevD.102.063008)
- Margueron, J., Hoffmann Casali, R., & Gulminelli, F. 2018, *PhRvC*, 97, 025806, doi: [10.1103/PhysRevC.97.025806](https://doi.org/10.1103/PhysRevC.97.025806)
- Miao, Z., Li, A., Zhu, Z., & Han, S. 2020, *ApJ*, 904, 103, doi: [10.3847/1538-4357/abbd41](https://doi.org/10.3847/1538-4357/abbd41)
- Miller, M. C., Lamb, F. K., Dittmann, A. J., et al. 2019, *ApJL*, 887, L24, doi: [10.3847/2041-8213/ab50c5](https://doi.org/10.3847/2041-8213/ab50c5)
- . 2021, *ApJL*, 918, L28, doi: [10.3847/2041-8213/ac089b](https://doi.org/10.3847/2041-8213/ac089b)
- Montana, G., Tolos, L., Hanauske, M., & Rezzolla, L. 2019, *PhRvD*, 99, 103009, doi: [10.1103/PhysRevD.99.103009](https://doi.org/10.1103/PhysRevD.99.103009)
- Most, E. R., Weih, L. R., Rezzolla, L., & Schaffner-Bielich, J. 2018, *PhRvL*, 120, 261103, doi: [10.1103/PhysRevLett.120.261103](https://doi.org/10.1103/PhysRevLett.120.261103)
- Oertel, M., Hempel, M., Klähn, T., & Typel, S. 2017, *RvMP*, 89, 015007, doi: [10.1103/RevModPhys.89.015007](https://doi.org/10.1103/RevModPhys.89.015007)
- Paschalidis, V., Yagi, K., Alvarez-Castillo, D., Blaschke, D. B., & Sedrakian, A. 2018, *PhRvD*, 97, 084038, doi: [10.1103/PhysRevD.97.084038](https://doi.org/10.1103/PhysRevD.97.084038)
- Pereira, J. P., Flores, C. V., & Lugones, G. 2018, *ApJ*, 860, 12, doi: [10.3847/1538-4357/aabfbf](https://doi.org/10.3847/1538-4357/aabfbf)
- Pisarski, R. D., Skokov, V. V., & Tsvelik, A. 2019, *Univ*, 5, 48, doi: [10.3390/universe5020048](https://doi.org/10.3390/universe5020048)
- Raaijmakers, G., Greif, S. K., Hebeler, K., et al. 2021, *ApJL*, 918, L29, doi: [10.3847/2041-8213/ac089a](https://doi.org/10.3847/2041-8213/ac089a)
- Rau, P. B., & Sedrakian, A. 2022, arXiv e-prints, arXiv:2212.09828. <https://arxiv.org/abs/2212.09828>
- Reed, B. T., Fattoyev, F. J., Horowitz, C. J., & Piekarewicz, J. 2021, *PhRvL*, 126, 172503, doi: [10.1103/PhysRevLett.126.172503](https://doi.org/10.1103/PhysRevLett.126.172503)
- Reinhard, P.-G., Roca-Maza, X., & Nazarewicz, W. 2021, *PhRvL*, 127, 232501, doi: [10.1103/PhysRevLett.127.232501](https://doi.org/10.1103/PhysRevLett.127.232501)
- Rezzolla, L., Most, E. R., & Weih, L. R. 2018, *ApJL*, 852, L25, doi: [10.3847/2041-8213/aaa401](https://doi.org/10.3847/2041-8213/aaa401)
- Riley, T. E., Watts, A. L., Bogdanov, S., et al. 2019, *ApJL*, 887, L21, doi: [10.3847/2041-8213/ab481c](https://doi.org/10.3847/2041-8213/ab481c)
- Riley, T. E., Watts, A. L., Ray, P. S., et al. 2021, *ApJL*, 918, L27, doi: [10.3847/2041-8213/ac0a81](https://doi.org/10.3847/2041-8213/ac0a81)
- Rodriguez, M. C., Ranea-Sandoval, I. F., Mariani, M., et al. 2021, *JCAP*, 02, 009, doi: [10.1088/1475-7516/2021/02/009](https://doi.org/10.1088/1475-7516/2021/02/009)
- Sedrakian, A., Li, J.-J., & Weber, F. 2021, arXiv e-prints, arXiv:2105.14050. <https://arxiv.org/abs/2105.14050>
- Sedrakian, A., Weber, F., & Li, J. J. 2020, *PhRvD*, 102, 041301, doi: [10.1103/PhysRevD.102.041301](https://doi.org/10.1103/PhysRevD.102.041301)
- Sieniawska, M., Turczanski, W., Bejger, M., & Zdunik, J. L. 2019, *A&A*, 622, A174, doi: [10.1051/0004-6361/201833969](https://doi.org/10.1051/0004-6361/201833969)
- Tan, H., Dexheimer, V., Noronha-Hostler, J., & Yunes, N. 2022, *PhRvL*, 128, 161101, doi: [10.1103/PhysRevLett.128.161101](https://doi.org/10.1103/PhysRevLett.128.161101)
- Tan, H., Dore, T., Dexheimer, V., Noronha-Hostler, J., & Yunes, N. 2022, *PhRvD*, 105, 023018, doi: [10.1103/PhysRevD.105.023018](https://doi.org/10.1103/PhysRevD.105.023018)
- Tang, S.-P., Jiang, J.-L., Han, M.-Z., Fan, Y.-Z., & Wei, D.-M. 2021, *PhRvD*, 104, 063032, doi: [10.1103/PhysRevD.104.063032](https://doi.org/10.1103/PhysRevD.104.063032)
- Tews, I., Margueron, J., & Reddy, S. 2018, *PhRvC*, 98, 045804, doi: [10.1103/PhysRevC.98.045804](https://doi.org/10.1103/PhysRevC.98.045804)
- Zdunik, J. L., Bejger, M., Haensel, P., & Gourgoulhon, E. 2008, *A&A*, 479, 515, doi: [10.1051/0004-6361:20078346](https://doi.org/10.1051/0004-6361:20078346)
- Zdunik, J. L., & Haensel, P. 2013, *A&A*, 551, A61, doi: [10.1051/0004-6361/201220697](https://doi.org/10.1051/0004-6361/201220697)
- Zhang, N.-B., & Li, B.-A. 2021, *ApJ*, 921, 111, doi: [10.3847/1538-4357/ac1e8c](https://doi.org/10.3847/1538-4357/ac1e8c)
- Zhang, N.-B., Li, B.-A., & Xu, J. 2018, *ApJ*, 859, 90, doi: [10.3847/1538-4357/aac027](https://doi.org/10.3847/1538-4357/aac027)